Combined experimental and theoretical study of field and current conditioning in magnetically shielded superconducting films

Ch. Jooss and E. Brinkmeier
Institut für Materialphysik, Friedrich-Hund-Platz 1, 37077 Göttingen, Germany

H. Heese
Institut für Numerische und Angewandte Mathematik, Lotzestrasse 16-18, 37083 Göttingen, Germany
(Received 3 April 2005; revised manuscript received 8 July 2005; published 19 October 2005)

Via magneto-optical imaging of flux density distributions it is shown that the flux-free Meissner state in thin film superconductors can be stabilized towards higher external fields and higher transport currents by using soft magnetic environments. A theoretical understanding of this effect is developed by applying a theoretical model of the Meissner state of thin superconducting strips in magnetic environments. The calculated magnetic field profiles agree well with those derived experimentally for a variety of shielding configurations. It is shown that the current density distributions in the superconducting films are modified by the presence of the soft magnets. Locally, large overcritical values of the current density can be obtained. Moreover, it is demonstrated that magnetic shielding also works for the stabilization of the Meissner phase of grain boundaries in high-temperature superconductors. Since magnetic flux strongly decreases the critical current density across grain boundaries, this effect has particular importance for the improvement and understanding of the current transport in granular superconductors.

DOI: 10.1103/PhysRevB.72.144516 PACS number(s): 74.25.Qt, 74.78.Bz

I. INTRODUCTION

In type-II superconductors, the mechanisms of loss-free current transport in the Meissner phase completely differ from the Shubnikov phase. In the Meissner phase, the current density is flowing at the surface of the sample in order to shield the interior of the superconductor from magnetic field penetration. The maximum value of the current density in this case is given by the depairing current density j_0 which is usually at least one order of magnitude larger than the highest critical current density j_c in the Shubnikov phase.[1] In the latter, magnetic flux penetrates in the form of flux quanta into the volume of the superconductor. Since a current is able to induce flux motion via the Lorentz force and therefore electric losses, a loss-free current density requires the pinning of the flux at lattice defects in the crystal lattice of the material. Consequently, the critical current density j_c is determined by the pinning strength of the lattice defects and simultaneously limited by thermally activated depinning.

Since Meissner currents are restricted to the surface area of a superconductor, a volume current transport can be realized in the Shubnikov phase only. However, this is different in thin film superconductors with thickness $d \leqslant \lambda$, where λ denotes the London magnetic penetration depth of a magnetic field in the Meissner phase. In this case, the Meissner current can flow in a large part of the cross section of the specimen. In contrast to bulk samples, where the Meissner phase is stable in external magnetic fields up to the lower critical field of the material H_{c1}, large magnetic stray fields in thin films give rise to magnetic flux entry even for external fields $H_{ex} < H_{c1}$. The effective field of first flux penetration H^* tends to 0 for $d \to 0$.[2] The same problem arises for a transport current in the Meissner phase which exhibits large stray field peaks at the edges of the thin film sample. Therefore, it may be strongly desirable to find a way to prevent magnetic flux penetration into the film and to stabilize the Meissner phase towards higher external fields or stray fields of transport currents.

In recent years, theoretical ideas to modify the flux and current distribution in superconductors via the change of the magnetic environment of the sample have been developed.[3,4] Formulating the approach mathematically in a more generalized setting and using potential theory together with boundary integral equation methods, it has been demonstrated how mathematics can provide tools for efficiently and accurately approximating magnetic field and current distributions in both cases of external fields and transport currents.[5,6]

In an experimental study, it was shown that it is possible to shield the perpendicular component of the magnetic flux density by a soft magnetic material at the edges of the film.[7] The field range for the stabilization of the Meissner phase could be extended in $YBa_2Cu_3O_7$ (YBCO) films at $T=5$ K to external fields up to 164 mT. This has to be contrasted to the $H_{c1,c} \approx 45-90$ mT parallel to the c axis of the bulk YBCO material[8] and to effective penetration fields $H^* < 10$ mT in thin films (depending on the film's thickness). By the application of inversion schemes of Biot-Savart's law, the modified flux distributions have been interpreted in Ref. 7 to be related to overcritical current densities. For Fe-sheathed bulk MgB_2 wires it was found from magnetic flux profiles that transport currents can be redistributed by the presence of magnetic environments.[9] This effect was interpreted by the authors as an evidence for the presence of overcritical current densities.[10]

A somewhat different approach for the stabilization of a superconducting state by ferromagnetic environments was applied for low-T_c superconductors.[11,12] In that work, the local stray field of magnetic dots and magnetic domain walls

was utilized to locally reduce the magnetic field and thus to enhance the superconducting state at certain external magnetic fields. In contrast, the geometries of Ref. 7 and those in the present work are selected to totally prevent magnetic flux penetration from the edge of the superconducting sample.

In this paper, we directly compare magnetization and transport experiments in symmetrically and asymmetrically shielded YBCO thin films. We use bicrystalline films, where the grain boundary is utilized as an extremely sensitive detector for the presence of magnetic flux entry at the film's edges. The application of bicrystalline films allows the simultaneous investigation of two important issues: (i) The redistribution of flux and currents for a geometry of the strip with an approximately one-dimensional current distribution. This can be realized by analyzing the flux and current distribution at a well-suited position in the sample sufficiently away from the grain boundary. (ii) The effect of the magnetic environment on the flux and current distribution at the grain boundary. Here it is investigated whether magnetic shielding of flux can also be achieved for GBs, and, whether the stabilization of the Meissner phase in the grain boundary is related to a higher intergranular current transport.

In order to develop a detailed understanding of the observed effects, a mathematical model of a thin film superconducting strip with a one-dimensional current distribution is applied. This model is valid for magnetically screened superconducting layers in the Meissner state, where the magnetic environment is of arbitrary shape. Thus it renders a direct comparison with the observed flux density distributions possible as long as the films are in the Meissner state. Moreover, it allows the determination of intragranular Meissner currents and the analysis to be to some extent carried over to the related intergranular Meissner current distributions in the grain boundary of the superconductor film.

II. THEORY

In this section we consider a mathematical model for the Meissner state of a superconducting strip in a magnetically shielded environment in presence of either a homogeneous external magnetic field or a transport current. For this we assume that the strip and the soft magnets are infinitely long in the y direction with a constant cross section. All physical quantities do not depend on y and the y component of the magnetic self-field is zero. Additionally we either apply a homogeneous external magnetic field in positive z direction, i.e.,

$$\mathbf{H}_{ex} = (0,0,H_{ex})^T, \tag{1}$$

or we apply a nonzero transport current in the positive y direction. The superscript T indicates a transposed vector.

This section is organized as follows. First we will formally state the boundary value problems for the Laplace equation which form the heart of our model. After briefly discussing the issue of unique solvability for the boundary value problems we will describe in detail how they relate to the physical situation formulated in the previous paragraph. We will then give meaning to the geometric assumptions of the model as they are relevant for a comparison with experiments. Finally we will discuss various features of the presented model that will be used extensively in Sec. V where we present numerical simulations that have been computed with this model.

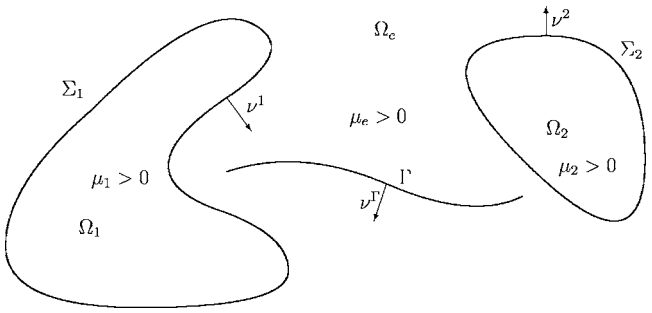

FIG. 1. Sketch of the cross section of a superconducting strip Γ in a magnetically shielded environment.

For the desription of our model let us now state the following boundary value problems for the Laplace equation.

Let Ω_1, Ω_2 be two bounded, simply connected domains in $\mathbb{R}^2$ with $\bar{\Omega}_1 \cap \bar{\Omega}_2 = \emptyset$ representing the cross sections of the shielding soft magnets. We assume that the boundaries Σ_1 of Ω_1 and Σ_2 of Ω_2 are of class C^2, define $\Omega_e := \mathbb{R}^2 \setminus (\bar{\Omega}_1 \cup \bar{\Omega}_2)$, and let ν^i be the unit normal to Σ_i directed into Ω_e. Let $\Gamma \subset \Omega_e$ be an arc of class C^3 representing the cross section of the superconducting strip, i.e., there exists $\gamma: [-1,1] \to \mathbb{R}^2$ three times differentiable, injective and regular such that $\Gamma = \gamma([-1,1])$. Furthermore, $\mu_e > 0$, $\mu_1 > 0$, and $\mu_2 > 0$ denote the magnetic permeabilities in the respective domains (see Fig. 1).

Now, in either case of a homogeneous external magnetic field or a transport current, we look for a real-valued function u that is continuous on $\mathbb{R}^2$ and twice continuously differentiable on $\mathbb{R}^2 \setminus (\Sigma_1 \cup \Sigma_2 \cup \Gamma)$ solving

$$\Delta u = 0, \quad \text{in } \Omega_e \setminus \Gamma, \tag{2}$$

$$\Delta u = 0, \quad \text{in } \Omega_i, \quad i = 1,2, \tag{3}$$

$$u = 0, \quad \text{on } \Gamma, \tag{4}$$

$$\frac{1}{\mu_e}\frac{\partial u_+}{\partial \nu^i} - \frac{1}{\mu_i}\frac{\partial u_-}{\partial \nu^i} = 0, \quad \text{on } \Sigma_i, \quad i = 1,2, \tag{5}$$

such that $\tilde{u}(x,z)$ is continuous and bounded on $\mathbb{R}^2$, and harmonic in $\Omega_e \setminus \Gamma$, Ω_1 and Ω_2, where

$$\tilde{u}(x,z) := u(x,z) - \mu_e H_{ex} x, \quad (x,z) \in \mathbb{R}^2 \tag{6}$$

for the case of an external field, or

$$\tilde{u}(x,z) := u(x,z) - \frac{\mu_e I}{2\pi|\Gamma|}\int_\Gamma \ln\frac{1}{|(x,z) - \mathbf{x}'|} ds(\mathbf{x}'), \tag{7}$$

for $(x,z) \in \mathbb{R}^2$ in the case of a transport current, respectively. Here $|\Gamma|$ denotes the length of Γ and I denotes the strength of the transport current.

We now turn to the issue of unique solvability for the two problems stated above noting that the problem for the trans-

port current case is exactly the one discussed in Ref. 6. For the case of a homogeneous external magnetic field it differs only by a different source term for u as given in Eq. (6). Hence, inspecting the analysis of Ref. 6 via integral equations, it can be seen that in each case there exists a unique solution u to each of the problems discussed above.

In the following we will justify that the uniquely determined solutions of the problems from above model the physical situation described at the beginning of the section. Defining

$$\mathbf{A} := [0, u(x,z), 0]^T, \quad (x,z) \in \mathbb{R}^2, \tag{8}$$

similar to the ansatz proposed in Ref. 4 and

$$\mathbf{B} := \operatorname{curl} \mathbf{A} = \left(-\frac{\partial u}{\partial z}, 0, \frac{\partial u}{\partial x} \right)^T, \tag{9}$$

we immediately see that the field $\mathbf{B}$ is independent of y and its y component vanishes. From the central equation of magnetostatics we find additionally that for the current density $\mathbf{j}$ we have

$$-\mu_0 \mathbf{j} = \operatorname{curl} \mathbf{B} = (0, -\Delta u, 0)^T. \tag{10}$$

Now Eqs. (2) and (3) tell that the exterior domain $\Omega_e \backslash \Gamma$ as well as the inside of the soft magnets Ω_1 and Ω_2 are current free. Moreover, we have that $\operatorname{div} \mathbf{B} = \operatorname{div} \operatorname{curl} \mathbf{A}$ vanishes entirely. Hence $\mathbf{B}$ is indeed a magnetic field and we can interpret $\mathbf{A}$ as a magnetic potential. Furthermore we know that at the interfaces Σ_1 and Σ_2 the magnetic field $\mathbf{B}$ has to satisfy

$$\mathbf{B}_+ \cdot \tilde{\nu}^i = \mathbf{B}_- \cdot \tilde{\nu}^i \tag{11}$$

$$\frac{1}{\mu_e} \mathbf{B}_+ \times \tilde{\nu}^i = \frac{1}{\mu_i} \mathbf{B}_- \times \tilde{\nu}^i \tag{12}$$

for $i = 1, 2$, where $\tilde{\nu}^i := (\nu_1^i, 0, \nu_2^i)^T \in \mathbb{R}^3$. Computing

$$\mathbf{B}_\pm \times \tilde{\nu}^i = \left(0, \frac{\partial u_\pm}{\partial x} \nu_1^i + \frac{\partial u_\pm}{\partial z} \nu_2^i, 0 \right)^T = \left(0, \frac{\partial u_\pm}{\partial \nu^i}, 0 \right)^T \tag{13}$$

using Eq. (9), we observe that Eq. (12) is satisfied using Eq. (5). Noting that $t^i := (\nu_2^i, -\nu_1^i)^T$ is the tangential vector to Σ_i we compute

$$\mathbf{B}_\pm \cdot \tilde{\nu}^i = \frac{\partial u_\pm}{\partial t^i}. \tag{14}$$

Consequently continuity of u implies Eq. (11). Similarly, we find that for ν^Γ being the unit normal to Γ and setting $\tilde{\nu}^\Gamma := (\nu_1^\Gamma, 0, \nu_2^\Gamma)^T \in \mathbb{R}^3$ we can compute

$$\mathbf{B}_\pm \cdot \tilde{\nu}^\Gamma = \frac{\partial u_\pm}{\partial t^\Gamma}, \tag{15}$$

where $t^\Gamma := (\nu_2^\Gamma, -\nu_1^\Gamma)^T$. Now Eq. (4) together with continuity of u implies that the normal component of the magnetic field vanishes at the surface of the superconducting strip, characterizing it thereby as being in the Meissner state. Finally, for the case of a homogeneous external magnetic field, by rearranging the representation (6) and using Eq. (9), we observe that the magnetic field $\mathbf{B}$ can be decomposed into

$$\mathbf{B} = \mu_e \mathbf{H}_{ex} + \operatorname{curl}(0, \tilde{u}, 0)^T = \mu_e \mathbf{H}_{ex} + O\left(\frac{1}{|x|} \right) \tag{16}$$

since $\tilde{u}$ is bounded at infinity. Similarly, for the case of a transport current, we find from Eq. (7) that

$$\mathbf{B} = O\left(\frac{1}{|x|} \right) \tag{17}$$

again by the boundedness of $\tilde{u}$ at infinity.

We will now discuss the relevance of the geometric assumptions that we have formulated in stating the boundary value problems. The domains Ω_1 and Ω_2 represent the cross sections of the shielding magnetic environment. The postulated boundedness means that we only consider finite geometries; the domains being simply connected is mainly to ensure that they have no holes. Openness and the regularity of the boundary contours Σ_1 and Σ_2 are purely technical assumptions that are required to make mathematical theory work. The boundary regularity ensures continuity of the normal to the boundary thereby ruling out the domains having corners. This is not a vital restriction for the comparison of the model with experiments in cases where the experimental geometry has corners since we can approximate corners sufficiently well by smooth boundary curves.

Similarly to the domains the arc Γ represents the cross section of the superconducting strip. The modeling of a thin volume sample by a one-dimensional strip is a well known approach (see Ref. 13). It being injective and smoothly parametrized from a closed interval is again a rather technical assumption that is required from the point of view of mathematical theory. However, this assumption also ensures that the cross section does not intersect with itself, does not form a closed curve, has finite length, and a continuous normal, i.e., the strip has no corners or cusps. The arc being parametrized from a closed interval and contained in the exterior domain Ω_e also ensures that there is no direct contact between the superconducting strip and the magnetic environment. We note that the model is certainly valid in the case where the cross section of the superconducting strip is a line segment, but that the geometric assumptions on the arc allow a much wider choice of geometries.

For the rest of this section we want to focus on several features of the model presented in Ref. 6 and its applications as described above. Above all we note that it is constructive, i.e., not only deduces the existence of a uniquely determined solution but also provides a representation of the solution as a combination of a single layer potential over Γ and double layer potentials over the contours Σ_1 and Σ_2.

This representation has three major advantages. First, it allows relatively simple approximations of the solution and its derivatives in all of $\mathbb{R}^2$. Thereby it provides efficient means for computing the magnetic field or any of its components. This allows the comparison of the method with experimental data that are derived, for example, from magneto-optical measurements. Secondly, the representation of the solution allows further physical interpretation. From the representation in Ref. 6 we see that the self-field of the superconducting strip is generated by a single layer potential of the form

$$(S_\Gamma\varphi)(\mathbf{x}) := \frac{1}{2\pi}\int_\Gamma \ln\frac{1}{|\mathbf{x}-\mathbf{x}'|}\left[\varphi(\mathbf{x}') - \frac{1}{|\Gamma|}\int_\Gamma \varphi\, ds\right] ds(\mathbf{x}'), \tag{18}$$

for $\mathbf{x} \in \mathbb{R}^2$, where $|\Gamma|$ again denotes the length of Γ. From the jump relations of the single layer potential (see Ref. 5) we find that

$$\frac{\partial}{\partial \nu^\Gamma}[(S_\Gamma\varphi)_- - (S_\Gamma\varphi)_+] = \varphi - \frac{1}{|\Gamma|}\int_\Gamma \varphi\, ds \tag{19}$$

since the double layer potentials over Σ_1 and Σ_2 are analytic across Γ. In terms of the magnetic field this reads

$$\mathbf{B}_-^{self}\cdot\vec{t}^\Gamma - \mathbf{B}_+^{self}\cdot\vec{t}^\Gamma = \varphi - \frac{1}{|\Gamma|}\int_\Gamma \varphi\, ds, \tag{20}$$

where $\vec{t}^\Gamma$ is defined as above. From Ref. 4 we know that the jump in the tangential component of the magnetic field on the surface of a superconducting strip corresponds to the current density of the superconducting strip. This means that the proposed mathematical model can also be used as a tool for directly computing the rearranged current distribution in the superconducting strip (or at least approximations to it). Third, the mathematical model can be used for prediction of field and current distributions. As the model in Ref. 6 is applicable to a wide range of geometries for the shielding soft magnets (and also for the superconducting strip, a feature we do not want to focus on here) it may be used to fit current and/or field distributions to certain optimizing criteria. In forthcoming papers we will propose a mathematically well founded optimization procedure, where the geometry of the shielding soft magnets is optimized with respect to the capacity of the superconducting strip for carrying transport currents or admitting high external magnetic fields, respectively.

III. EXPERIMENT

Superconducting c axis oriented $YBa_2Cu_3O_7$ (YBCO) thin films are grown on bicrystalline, 1 mm thick $SrTiO_3$ substrates with pulsed laser deposition. The deposition parameters are reported elsewhere.[14] For the magneto-optical imaging experiments with and without a soft magnetic environment, two different kinds of sample geometries are patterned by optical lithography and wet chemical etching: For the magnetization experiments, we use a square shaped film (sample A) with a lateral size of 3×3 mm^2, where a 4° [001] tilt boundary is located in the middle of the sample and oriented parallel to two of the sample's edges. For the transport experiments, we use two 420 μm and 500 μm wide tracks (samples B and C). Sample B has a 3° [001] tilt boundary, whereas sample C is single crystalline. All three films A-C have a thickness d of 300 nm.

The soft magnetic environment is realized with dense FeSi(3%) sinter material of a size of $2\times1.5\times12$ mm^3. At a temperature of $T=10$ K, the initial permeability of the bulk magnets is ≈80. The saturation field is larger than 1.5 T and could not be determined in our experiments. However, in the range of the values of the stray field of the superconducting films ($B_z=0-200$ mT) and the externally applied magnetic fields ($\mu_0 H_{ex}<50$ mT), the FeSi magnets exhibit an approximately linear response. For the magnetic screening experiments, the bulk soft magnets are put next to one of the edges of the superconducting film as shown in Fig. 2. A small distance $a\approx1$ μm between the surface of the soft magnet and the edge of the superconducting film is realized by a mounting which presses the STO substrate to the soft magnet sample.

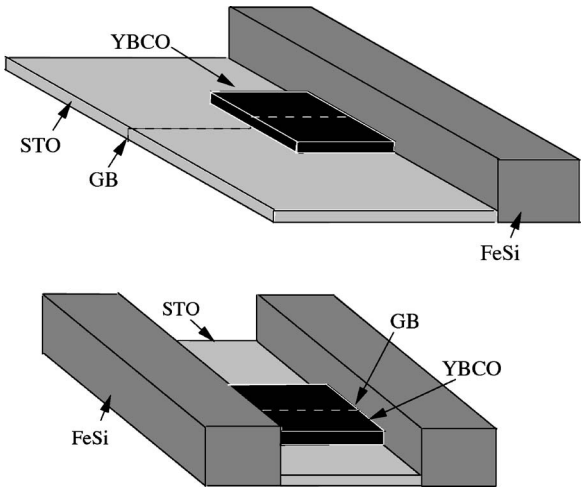

FIG. 2. Sketch of the experimental arrangement for the magnetic screening experiments at superconducting $YBa_2Cu_3O_7$ (YBCO) films and grain boundaries (GB). Two kinds of experiments are performed with either FeSi bulk magnets positioned at one edge [asymmetric-screening (AS) configuration] or at two opposite edges of the sample [symmetric-screening (SS) configuration]. Shown is the sample's geometry for magnetization experiments; for the transport experiments the YBCO square is replaced by a YBCO track.

The subsequent characterization of the flux density distributions is performed with a magneto-optical imaging technique, based on the Faraday effect in sensor layers which are put on top of the superconducting films. The field sensing iron garnet is observed via an advanced polarization microscope. Light intensity distributions representing the normal component of the flux density distribution $B_z(x,y)$ are recorded with a commercial charge-coupled device (CCD) camera using exposure times of 100 μs. The recorded gray scales are mapped to the local $B_z(x,y)$ values using a nonlinear calibration function which is determined separately for each sample. Current distributions can then be calculated using an inversion scheme for Biot-Savart's law.[15] In this paper the inversion scheme was only applied for superconducting films without soft magnetic environments in order to determine the critical current densities of the samples. In the experiments with soft magnetic screening, the values of the Meissner screening currents are estimated by comparison with the theoretical simulations. For the measured flux densities, a spatial resolution of approximately 1 μm is achieved.

Magneto-optical imaging of the flux distributions of the superconducting films is also performed while a transport

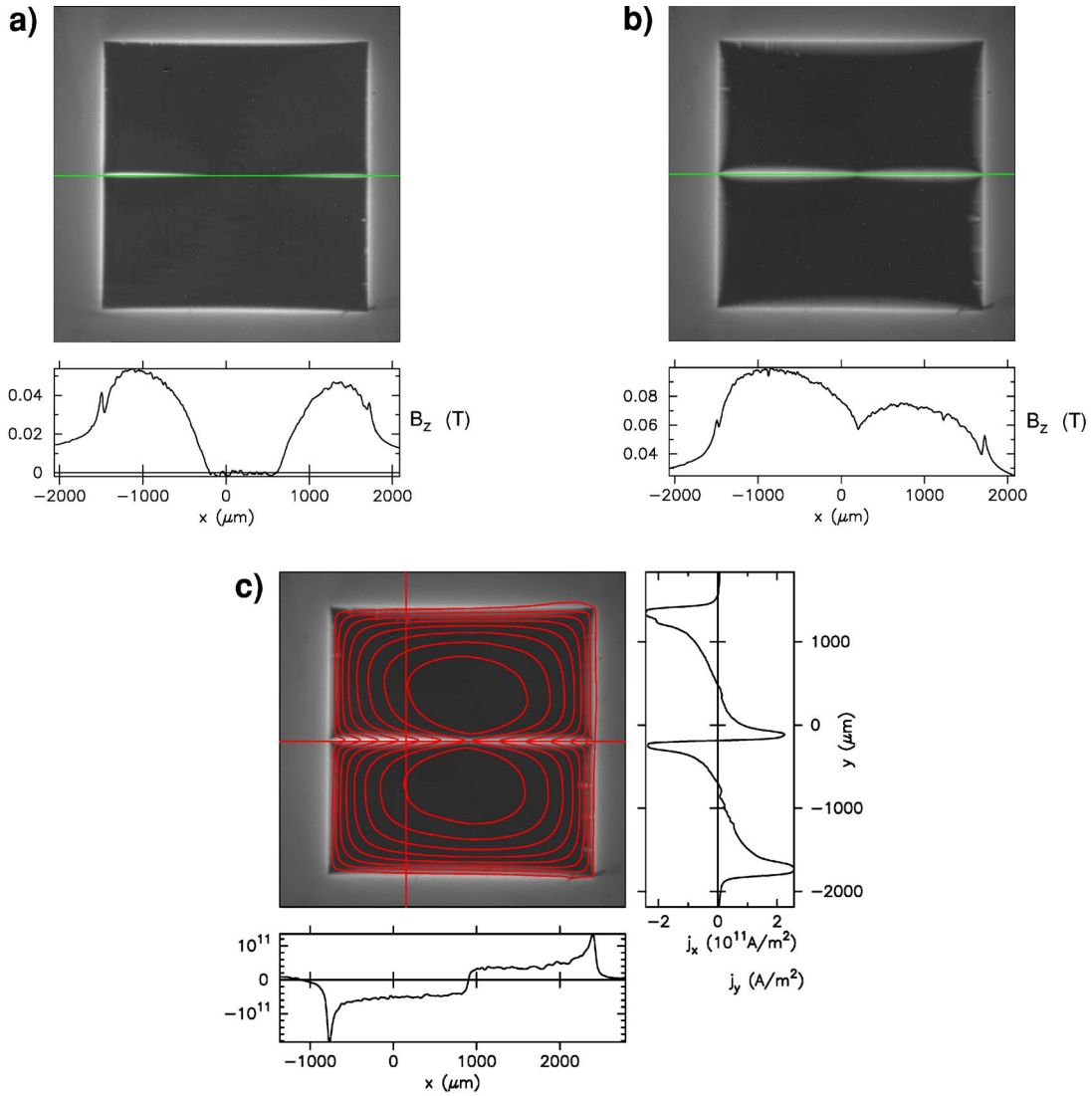

FIG. 3. (Color online) Flux density distributions of sample A with a 4° [001] tilt boundary. After zero-field cooling to $T=9$ K, an external magnetic field of $\mu_0 H_{ex}=13.2$ mT (a) and 26.4 mT (b) and (c) is applied normal to the film plane. (a) and (b) show the corresponding normal components of the flux density distribution $B_z(x,y)$ with a flux density profile at the position of the grain boundary (GB). Note that the asymmetry of the $B_z(x)$ profile along the GB is due to a slight tilt of the position of the line profile with respect to the GB plane. (c) shows the $B_z(x,y)$ distribution of (b) with superimposed current stream lines and current density profiles.

current was fed into the sample. In order to avoid heating effects at the contact pads for the current injection, the transport experiments are done in a pulsed current mode with pulse lengths between 100 μs and 1 s. The imaging of the field via the CCD camera is then triggered by the pulse.

IV. RESULTS

Figure 3 shows the magnetic flux penetration into the nonshielded square shaped YBCO film (sample A) with a 4° [001] tilt boundary after zero-field cooling to $T=9$ K and applying an external magnetic field normal to the film plane. Due to the large stray field of the thin film at the sample's edges, magnetic flux starts to penetrate into the film at an external magnetic field of $\mu_0 H_{ex}=\mu_0 H^* \approx 5$ mT, which is far below the first critical field $\mu_0 H_{c1}$. $\mu_0 H^*$ denotes the first penetration field of magnetic flux in the absence of magnetic shieldings. With increasing H_{ex} the penetration depth of the flux front increases and the size of the flux free Meissner area shrinks. This behavior is well known and can be described quantitatively in the framework of a thin film Bean model. A detailed discussion of the relevant flux and current distributions in thin films can be found in a review article.[16] The flux penetration is even more pronounced along the grain boundary (GB). This is not only due to the reduced current carrying capability of the GB but has also a geometrical reason: Due to the conservation of charge and the reduced current density j_{gb} across the GB, the current flow lines next to the GB are bent and thus produce an enhanced magnetic stray field at the location of the GB plane. Consequently, after the first flux has entered the GB, the related current distribution gives rise to a self-enhancement of the local flux and therefore to a self-enhanced flux penetration

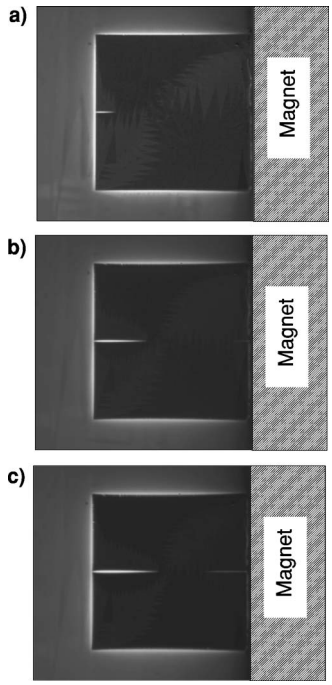

FIG. 4. Magnetization experiment with soft magnetic screening at the sample's left edge. The pictures show the $B_z(x,y)$ distribution of the same film as in Fig. 3 in external fields of 6.6 mT (a), 13.2 mT, (b), and 16.4 mT (c).

into the GB.[17] Therefore, in our experiments the GB serves as an extremely sensitive probe for the set-in of the flux penetration into the sample.

In order to demonstrate the effect of magnetic shielding by the presence of a bulk soft magnet, first the asymmetric-screening (AS) configuration was realized experimentally. A soft magnet was put next to only one edge of the sample. The magnetic flux distribution after cooling down in zero-external magnetic field (ZFC) to $T=9$ K and applying H_{ex} normal to the film plane is depicted in Fig. 4. In the AS configuration one can directly compare the normal flux penetration at the nonshielded edge with the modified behavior on the magnetically shielded edge of the film. As was already demonstrated,[7] the Meissner state is stabilized on the side with the magnet. Remarkably, this extension of the Meissner state in a higher field region is also valid for the GB.

A second series of experiments with the AS configuration was performed by applying a transport current to the superconducting film. Figure 5 shows the magnetic self-field distribution of a single crystalline YBCO strip after ZFC to $T=9$ K and applying a current of 20 A. The observed positive and negative flux density peaks are typical for transport currents in thin films[16] and reflect the large self-field concentration at the edges of the sample. The large values of the field at the sample's edges are the main reason that a current carrying Meissner state becomes unstable towards a current carrying state which is determined by flux pinning. The transition of a pure Meissner state into a state with gradually penetrating flux happens at a relatively small total current I^* far below the critical current I_c of the sample.

Figure 6 shows a series of magneto-optical images of the flux density distribution of a bicrystalline YBCO strip with a

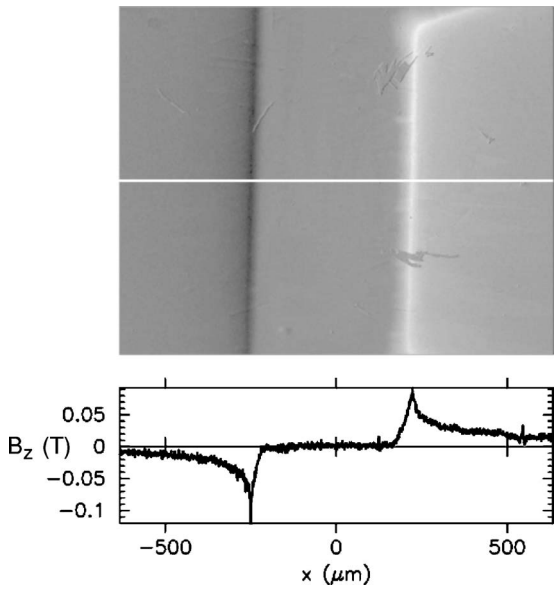

FIG. 5. Transport experiment using a single crystalline YBaCuO strip. The picture shows the $B_z(x,y)$ distribution of the strip in zero external field and with a transport current of $I=20$ A.

3° [001] tilt boundary for different transport currents. In this AS configuration, the penetration of the magnetic self-field into the right-hand side of the strip is completely suppressed up to the highest transport current realized in our experiments. In contrast, the flux penetration on the left-hand side of the strip (without soft magnetic environment) is not altered. A particular difficulty of that kind of experiment is the presence of high Lorentz and magnetostatic forces in the combined system of the superconductor, the magnet and the field sensing indicator film. Therefore, all components have to be mounted mechanically with high stability on top of the cooling plate of the cryostate. While cooling down this gives rise to compressive strain in the indicator film and therefore to an additional, irregular stripelike distortion of the contrast which is an artefact of the measurement. Nevertheless, the magnetic flux density distribution can be calibrated in this state and gives correct values. Figure 7 shows calibrated flux density profiles across the square and the strip for the magnetization and the transport experiment in the AS configuration, respectively. The profiles are taken at a well-suited position away from the GB, where the current distribution in the sample is approximated sufficiently well by a one-dimensional distribution $j_y(x)$.

Figure 8 shows flux density profiles for the same experiments as in Fig. 7. However, the profiles are taken at the position of the GB. In the magnetization experiment, the flux penetration at the GB starts at a penetration field of $\mu_0 H_{gb}^{*s} = 9.9 \pm 1$ mT at the magnetically shielded side, in comparison to $\mu_0 H_{gb}^{*} = 2 \pm 1$ mT at the nonshielded side. Furthermore, even after the flux has started to penetrate into the GB, the values of the penetration depth of the flux front and the stray fields are much smaller at the shielded side. This behavior is even more pronounced for the transport experiment. With increasing transport current I, the penetration depth of the flux front and the values of the stray fields increase by degrees at the nonshielded side. In contrast, no flux penetration

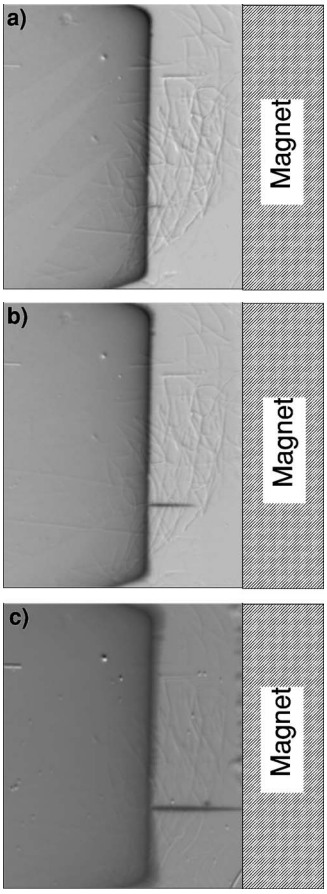

FIG. 6. Transport experiments using a bicrystalline YBaCuO strip with a 3° [001] tilt boundary and a soft magnetic screening at the sample's left edge. The pictures show the $B_z(x,y)$ distribution of the strip in zero external field and transport currents of $I=8$ A (a), 13.2 A (b), and 18.4 A (c).

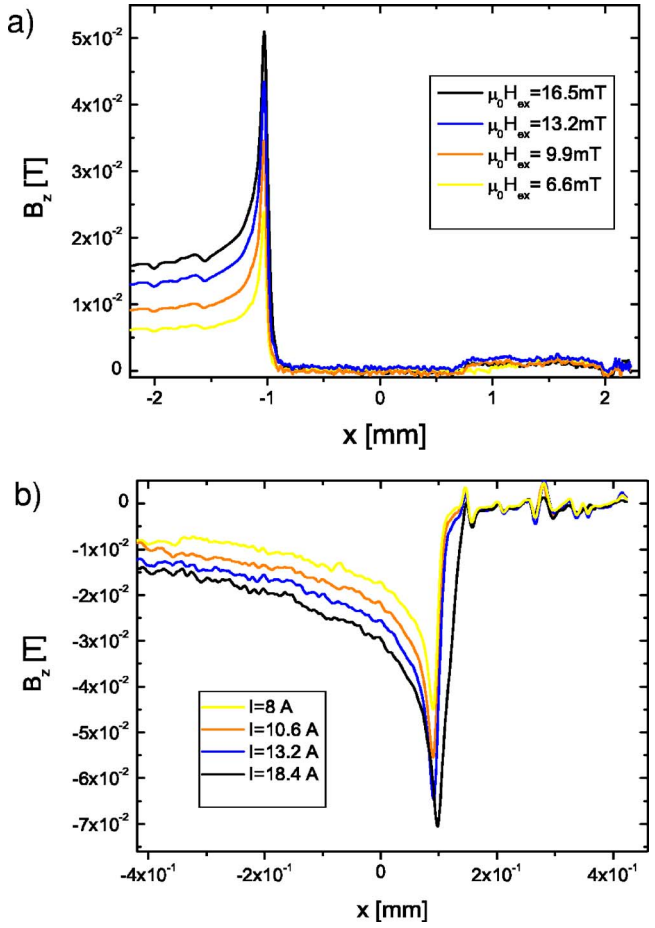

FIG. 7. (Color online) Profiles of the flux density $B_z(x)$ in a magnetization (a) and a transport experiment (b). The profiles are taken from the distributions in Fig. 4(a) and Fig. 6(b) at a position away from the GB.

is observed at the magnetically screened side. At the maximum transport current of $I=18.4$ A the GB is in a fully penetrated state. However, from the evolution and the shape of the flux profiles in Fig. 8, there is no indication that the flux has entered the GB from the right hand (shielded) side.

For comparison, Fig. 9 shows a magnetization experiment in the symmetric-screening (SS) configuration, where two soft magnets were positioned at the sample's left and the right edges. This experiment proves that a symmetric shielding of the film and also of the GB can be achieved. In this SS configuration the first penetration field for the GB is $H_{gb}^{*s}=9\pm1$ mT and does not significantly change in comparison to the AS configuration. In Fig. 9 the flux density distribution between the magnets for a lateral position outside the superconducting film is depicted. These profiles show that the soft magnets give rise to a significant weakening of the local magnetic field at the superconductor's left and right edge. For $\mu_0 H_{ex}=6.6$ mT, the local field B_z^{se} at the shielded edges of these samples is still below the measurement limit, whereas the local field peak at the nonshielded edge reaches $B_z^e=25$ mT. At $\mu_0 H_{ex}=16.5$ mT, $B_z^{se}\approx 2$ mT which is far below the first penetration field of the grain, however, it reaches the first penetration field of the GB.

V. NUMERICAL SIMULATIONS FOR SELECTED GEOMETRIES

In this section we present numerical simulations of the model described in Sec. II for the relevant geometries realized in the experiments. For both magnetizing and transport experiments we investigate the behavior of the B_z distribution in an asymmetrically shielded environment.

The geometric setup for the simulations is chosen to reflect the experimental setup from Sec. III. The reader has to bear in mind that the mathematical model from Sec. II deals with a two-dimensional cross section of the three-dimensional setup described in Sec. III. For the transport experiments the geometry of the superconducting strip Γ is assumed to be a line segment of length 0.42 mm, for the magnetizing experiment its length is 3 mm. In both cases the line segment is parallel to the x axis and centered at the origin. The geometry of the soft magnet Ω is a smooth approximation to a rectangle of width 2 mm and height 1.5 mm centered at the point $(1.421,-0.25)^T$ for the transport experiments, or $(2.501,-0.25)^T$ for the magnetizing experiments [in units of mm with respect to the (x,z) plane]. We realize this by accordingly stretching and shifting the closed analytic

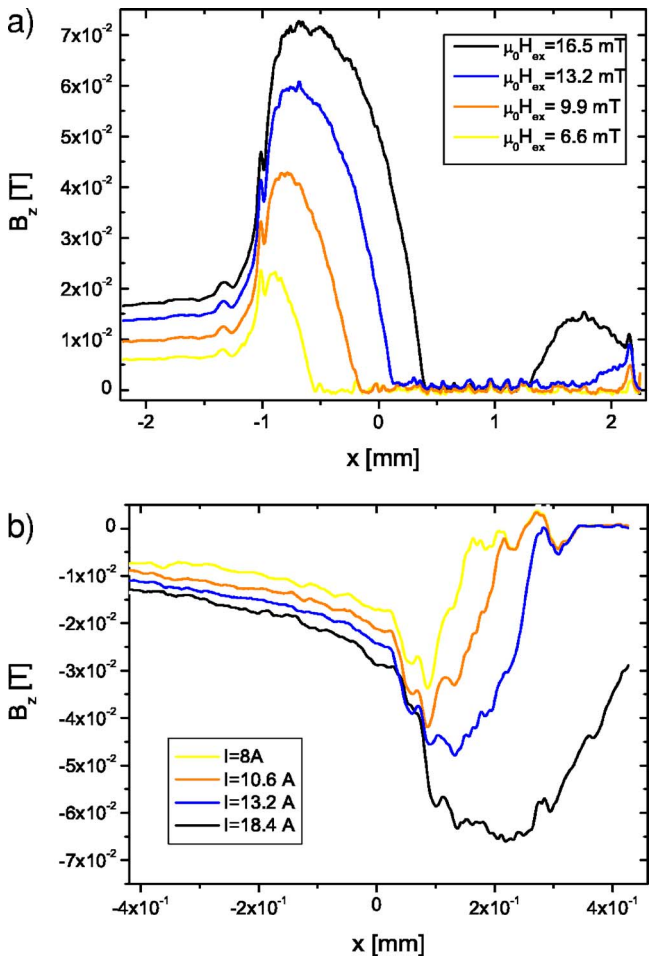

FIG. 8. (Color online) Profiles of the flux density $B_z(x)$ at the position of the grain boundary in the magnetization (a) (Fig. 4) and the transport experiment (b) (Fig. 6).

curve $x^{10}+z^{10}=1$ representing the boundary curve Σ. As mentioned in Sec. II this smooth approximation is essential for mathematical theory on which the simulations are based. The effect of it is to round the corners of the rectangle thereby also avoiding the development of singularities in the magnetic field at the corners which are predicted from physical theory.

The permeability of the soft magnet is 80, the permeability of the exterior domain is 1.

The numerical simulations have been performed using 512 nodes on the closed contour representing the boundary of the soft magnet, and 129 nodes on the line segment representing the superconducting strip. The effective gap between the superconducting strip and the boundary of the soft magnet is 1 μm.

The simulations are derived as follows. As described in Ref. 6, Sec. IV, the underlying system of integral equations is discretized using trigonometric interpolation and quadrature rules [see Ref. 6, Eq. (35)]. This results in a finite-dimensional linear system with in our case 641 variables which is solved directly. The variables form a discrete approximation to the densities of the ansatz functions for the solution u from Sec. II. The evaluation of the magnetic potential and the magnetic field is then realized by discretizing the ansatz function in the same way as the system of integral equations.

The current distributions in the superconducting strip [Figs. 10(b) and 11(b)] are a by product of these computations in the following sense. In Eq. (20) we have identified one of the defining densities of the ansatz function for the solution u as the current distribution in the superconducting strip. Hence we can read off a discrete approximation to it as one part of the solution to the finite-dimensional linear system that has been computed in order to evaluate the magnetic field and the magnetic potential.

Since the superconducting strip has zero thickness the obtained current density represents a sheet current density $J(x)$ in units of A/m. Formally, the current distributions and hence the magnetic field develop singularities at the endpoints of the superconducting strip. These singularities are treated adequately within the model. As to the graphical output, due to the discretization of the superconducting strip the current profiles are shown only up to a distance of 450 nm to the endpoints of the strip in the case of the magnetizing experiments, and 65 nm in the transport experiment case, respectively.

Figures 10(a) and 11(a) show the $B_z(x)$ profiles for the asymmetrically shielded magnetization and transport configurations realized in the experiments. They are directly comparable to Fig. 7. The one-dimensional $B_z(x)$ profiles are computed at a line parallel to the superconducting strip at a distance of 1 μm above the strip, where the field is nonsingular. This measurement distance in the simulations corresponds to the measurement distance in the magneto-optical measurements. The field is evaluated at 429 points, the spacing of which is chosen such that we have a fine resolution near the endpoints of the superconducting strip where the magnetic field displays an almost singular behavior, and a comparably low resolution away from the endpoints of the strip where the magnetic field is smooth. In our simulations we have realized such a distribution by subjecting equidistantly spaced points to a cosine transformation.

For the two-dimensional plots of the B_z distribution (Fig. 12) we use a grid of 429×400 points, where the points are equidistantly spaced in z direction, but again subject to the above-mentioned cosine transformation in x direction. The grid is chosen such that an evaluation of the field in the singularity is avoided. Since the main interest lies in the behavior of the field in the vicinity of the superconducting strip we have truncated the values of the B_z distribution at ±100 mT for the magnetizing experiment and at ±30 mT for the transport experiment. The superimposed field lines are isocontours of the corresponding magnetic potential, that is computed in the model as the solution u (see Sec. II). The plots contain 70 contours of the potential on a linear scale.

VI. DISCUSSION

In the following, the magnetic field conditioning as revealed by our experiments and simulations is discussed, and the theoretical and experimental results are compared. This section is organized as follows: (i) We compare the theoretical and experimental magnetic flux profiles at positions far

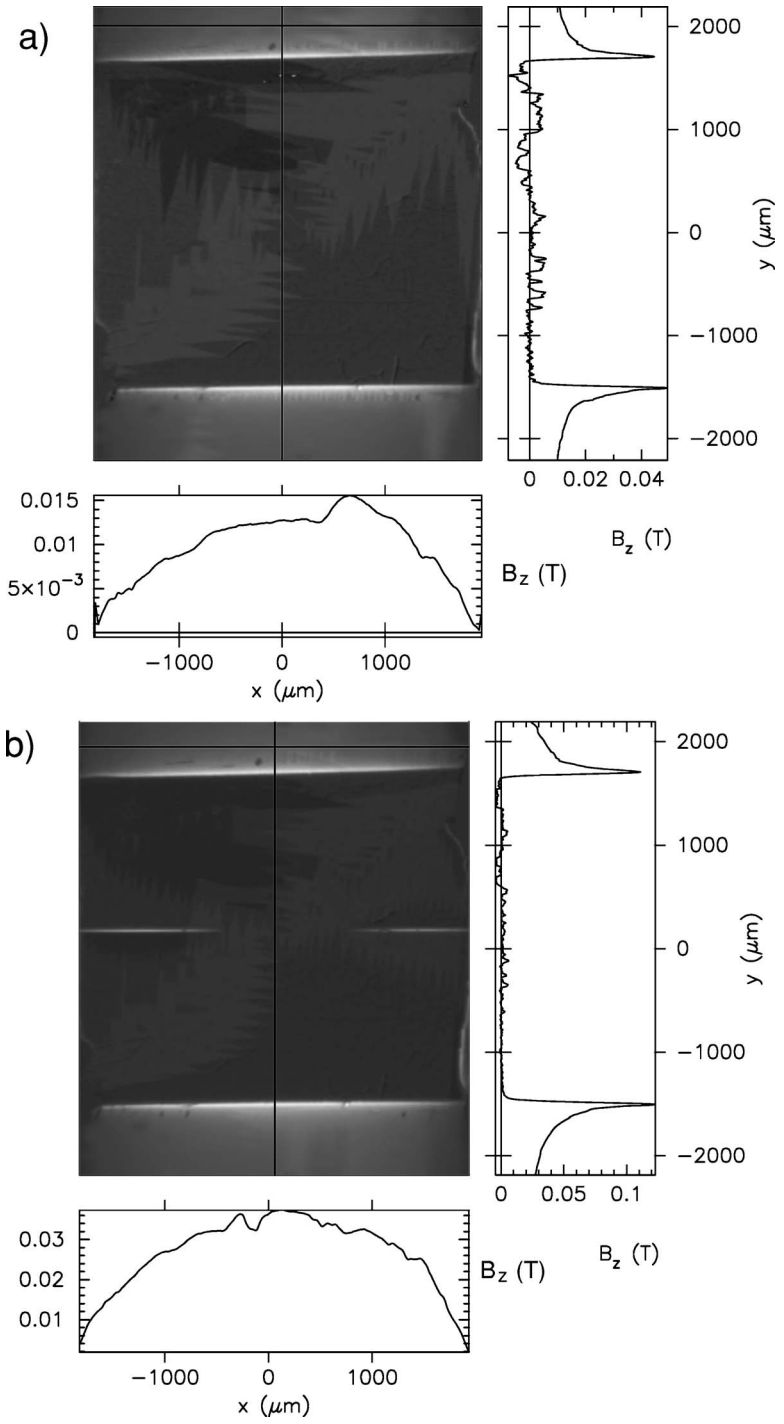

FIG. 9. Flux density distribution for the bicrystalline, symmetrically shielded YBCO film with a 4° [001] tilt boundary in a magnetization experiment. In this experiment two FeSi magnets are present on the sample's left and right edge. An external magnetic field of $\mu_0 H_{ex}$=6.6 mT (a) and 16.5 mT (b) is applied after zero-field cooling. The flux density profiles are taken at the positions of the lines in the images.

away from the GB. (ii) the intragrain Meissner current density due to the stabilization of the Meissner state is compared to the critical current density in the flux penetrated state (without shielding). (iii) We derive some conclusions for the current transport across the GBs in the Meissner and the flux penetrated state.

First, we start with a discussion of the qualitative behavior of the flux patterns. The comparison of the experimentally observed flux density profiles in Figs. 7(a) and 7(b) with the results of the simulations in Figs. 10(a) and 11(a) shows that the asymmetric shielding configurations are described appropriately in the framework of our model both in the magnetization and in the transport experiments. On the nonshielded left-hand edge of the film, the transport or magnetization currents generate large peaks in the flux density B_z. In the case of the magnetization experiments these local B_z^e values are several times larger than the external field. The large B_z^e values give rise to a break down of the Meissner state at the nonshielded left-hand edge and to the onset of flux penetration with a nucleation of the Shubnikov phase at the edge of the sample. In contrast to this behavior, the flux penetration is suppressed at the magnetically shielded edge up to much higher magnetic fields. The simulations in Figs. 10(a) and 11(a) show a significant suppression of the B_z peak at the

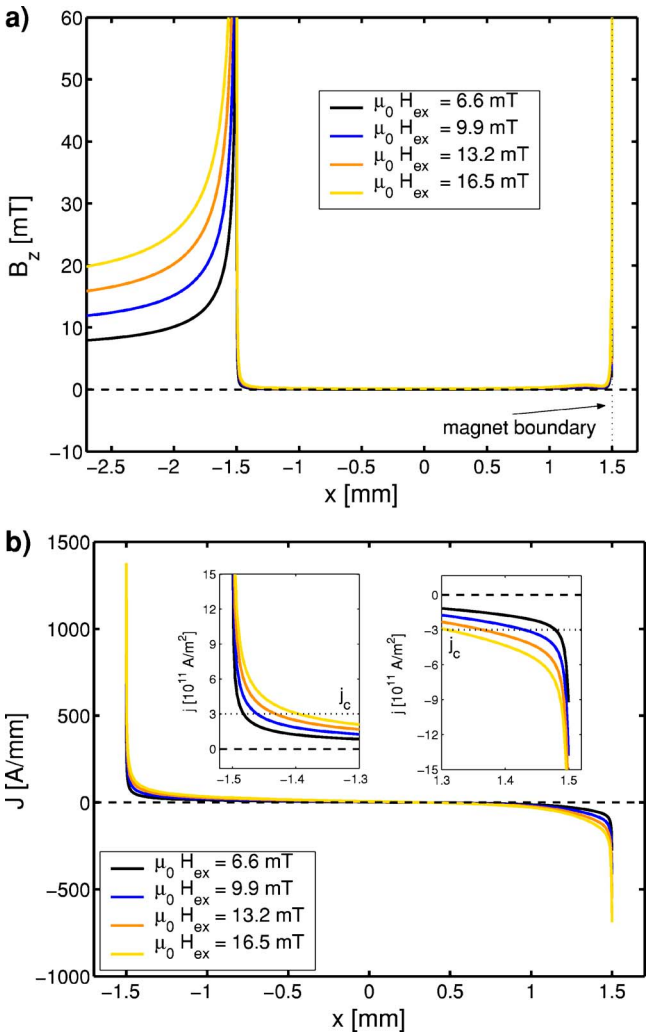

FIG. 10. (Color online) (a) Calculated $B_z(x)$ profiles of a superconducting strip in a magnetizing experiment when shielded on the right-hand side by a soft magnet with $\mu=80$ at distance of 1 μm from the edge of the strip. The experimental parameters correspond to the experiment shown in Figs. 4 and 7(a). (b) Sheet current profiles of a superconducting strip corresponding to the field profiles in (a). The insets show the current density $j(x)=J(x)/d$ at the sample's left and right edge. The j_c line indicates the experimental value of the critical current density for sample A.

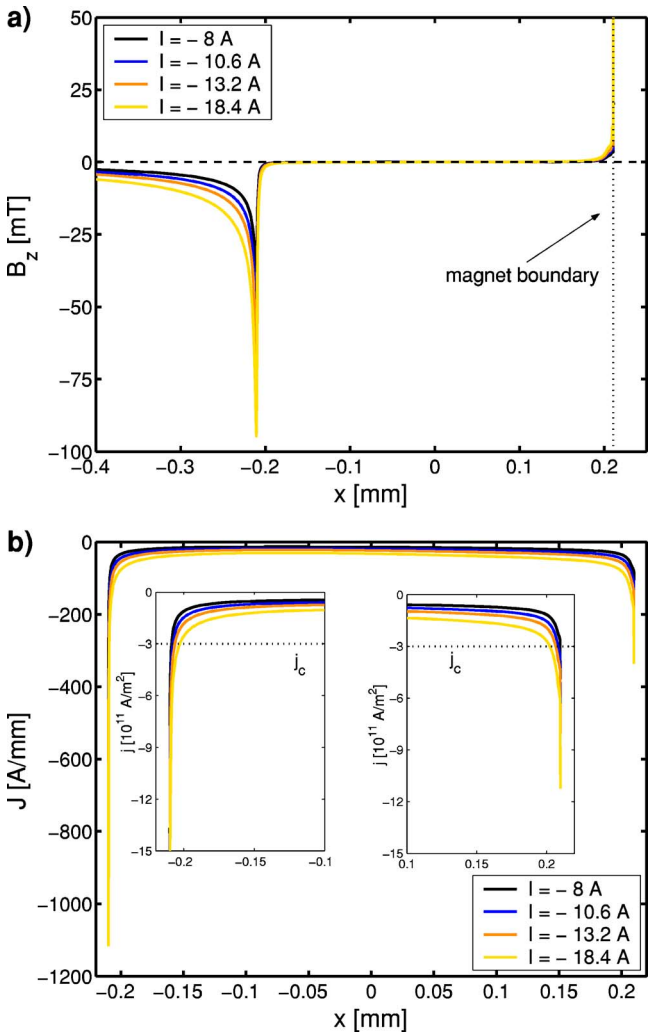

FIG. 11. (Color online) (a) Calculated $B_z(x)$ profiles of a superconducting strip in a transport experiment when shielded on the right-hand side by a soft magnet with $\mu=80$ at a distance of 1 μm from the edge of the strip. The experimental parameters correspond to the experiment shown in Figs. 6 and 7(b). (b) Sheet current profiles of a superconducting strip in the transport experiment corresponding to the field profiles in (a). The insets show the current density $j(x)=J(x)/d$ at the sample's left and right edges. The j_c line indicates the experimental value of the critical current density for sample B.

shielded edge B_z^{se} by factors of more than 10 due to the soft magnet.

The two-dimensional distribution of the $B_z(x,z)$ values in combination with the magnetic field lines of **B** as shown in Fig. 12 visualize the role of the soft magnet for the redistribution of the magnetic field: Its main effect is to diminish the magnetic flux at the edges of the superconducting film by concentrating the magnetic flux in the high-μ region. This is irrespective of B_z^{se} being generated by a transport or a magnetization current and thus works both in magnetization and in transport experiments.

Since the theoretical model describes infinitely thin films, a direct quantitative comparison between the flux distributions of the theory [Figs. 10(a) and 11(a)] with the results of the experiments [Figs. 7(a) and 7(b)] is only possible at positions, where the field singularities at the superconducting film edges are avoided. Outside the superconductor, the asymptotic behavior of $B_z(x)$ for $x \ll x_e$ (where x_e denotes the left, nonscreened edge of the superconductor) agrees nicely within an accuracy of $\approx 30\%$. Note that there is no free parameter in the theoretical simulations.

We now continue with the discussion of the current density distributions in the theoretical simulations and draw conclusions as to what extent they correspond to the experimental ones. The current distributions in Figs. 10(b) and 11(b) for the magnetization and the transport configurations, respectively, show that a significant redistribution of the Meissner current density is obtained. This was already suggested[4] for superconducting films next to symmetrically

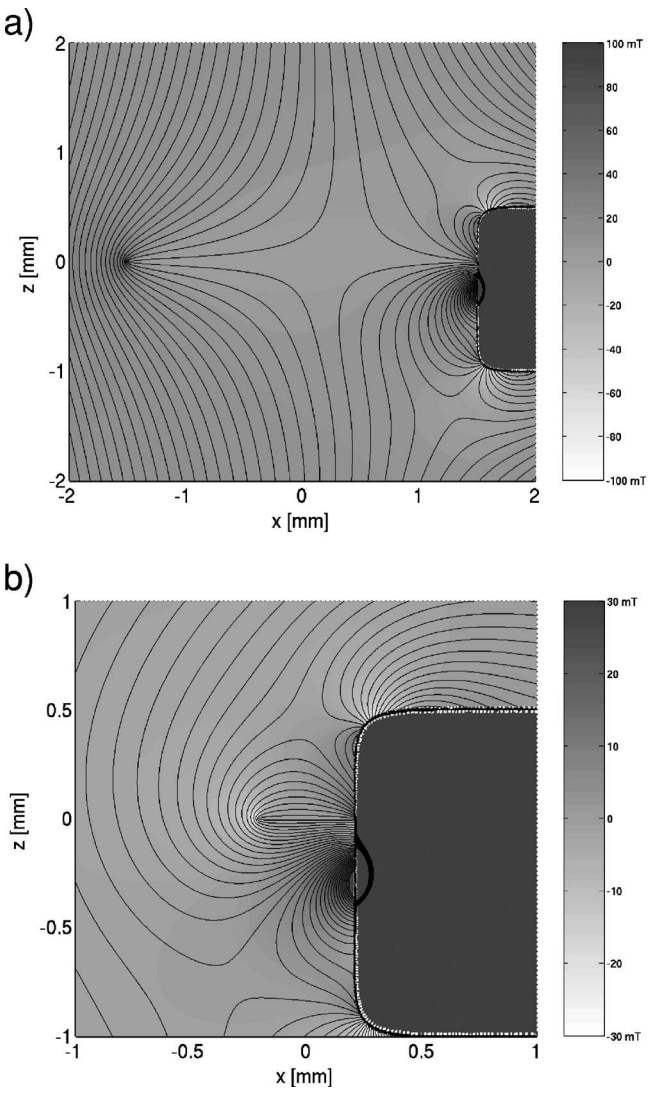

FIG. 12. (a) Calculated $B_z(x,z)$ distributions (scales) together with the field lines of **B** of a superconducting strip in the AS configuration. The external field in this magnetization experiment is $\mu_0 H_{ex}=16.5$ mT. The field is shown in the (x,z) plane of the superconductor-magnet arrangement. (b) The same as (a) but for the transport experiment with a current of $I=18.4$ A.

arranged soft magnetic half spaces. Now, it is proven for truly finite systems. The main modifications of the current distribution are a decrease of the peak of the current density at the edge next to the magnet, a redistribution with a slight increase of the Meissner current density towards the interior of the film, and a shift of the plane of symmetry of the magnetization current density $[x(J=0)]$ into the direction of the magnet. This result agrees nicely with the one of Ref. 4 (see Figs. 1 and 2).

For the interpretation of our results two characteristic values for current densities have to be taken into account which we will recall in the following: (i) The numerics nicely reproduce the well-known shape of Meissner screening currents $J(x) \propto [(W/2)^2 - x^2]^{1/2}$ in thin films without magnetic environments.[18] In general, the edge singularity for the current density has to be eliminated by a physical cutoff, given by the Ginzburg-Landau depairing current density $j_0 = \Phi_0/(3\sqrt{2}\pi\mu_0\xi_{ab}\lambda_{ab}^2)$, where Φ is the magnetic flux quanta, ξ_{ab} the coherence length in the (a,b) plane, and λ_{ab} the magnetic penetration depth. Using the material parameters of YBCO one obtains a characteristic value of $j_0 \approx 3.2 \times 10^{12}$ A/m^2. In Figs. 10(b) and 11(b) this cutoff corresponds to a sheet current of $J(x)=j(x)d=1060$ A/mm, where d denotes the thickness of the film. This sets an upper limit for the local current density which flows in the Meissner state. (ii) In contrast, after set-in of magnetic flux penetration and break down of the Meissner state at the film edge, the maximum current density of the superconducting films is limited by the pinning strength of material defects on flux lines. This defines a second characteristic current density, the critical current density j_c. In our experiments, the three films (A-C) have intragranular j_c values between 2.8×10^{11} A/m^2 [sample A, see Fig. 3(c)] and 3.2×10^{11} A/m^2 at $T=9$ K (samples B and C).

With the help of these characteristic values we can now draw conclusions on the relations between the Meissner current densities in the theoretical simulations and the experiments. Figures 10(b) and 11(b) reveal on the one hand that j remains below j_0 in the whole area of the superconducting film that is displayed, so the values of j on the shielded edges of the superconducting films are not an artefact of the model. On the other hand we observe by comparing the Meissner current distributions obtained by the simulations with the j_c values in the films [see insets of Figs. 10(b) and 11(b)] that $j > j_c$. From this we deduce that also in the experiments the current densities at the shielded edges of the film, where the Meissner state is stabilized, are overcritical. The result of Ref. 7, which was obtained by inversion of Biot-Savart's law, stating that overcritical values of up to $j/j_c \approx 4$ can be achieved is confirmed in Fig. 10(b), where j/j_c is up to 7 for the magnetization experiment. For the transport experiment a ratio of $j/j_c=3.3$ is observed at $I=18.4$ A. Since no breakdown of the Meissner state at the shielded edge is observed in the range of applicable transport currents $0 \leqslant I \leqslant 20$ A in our setup, we suggest that even larger ratios for overcritical transport current densities are possible.

Finally, we analyze how conclusions with respect to the magnetic shielding of grain boundaries and the potential for the improvement of current densities across grain boundaries can be drawn from the presented model. On first glance the model does not seem appropriate to study grain boundaries, since the simulations of the current distributions in magnetically shielded superconductors are restricted to the case of one-dimensional current distributions, whereas the description of a grain boundary requires complex two-dimensional current distributions. However, a formation of a convex $2d$ current pattern can be detected in our experiments because it is directly related to the generation of a significant magnetic stray field with a local maximum located at the position of the GB plane. Such two-dimensional patterns are only present if $j_{gb} < j$, where j is the current density in the grain, i.e., when flux starts to penetrate into the GB on the shielded side of the film. In contrast to that, the observed absence of a magnetic flux density in the GB plane for $H_{ex} \leqslant H_{gb}^*$ (or for transport currents below a critical value I^*) shows that $j_{gb} = j$. This suggests that the presented model which uses a one-

dimensional current density can be applied to the AS experiments, as long as no flux penetration in the GB is visible on the shielded side. Consequently, the current distributions in Fig. 10(b) for $H_{ex} \leqslant H_{gb}^{*s} = 9.9$ mT and in Fig. 11(b) for $I \leqslant I^*$, where $I^* \geqslant 18.4$ A, can be utilized to obtain an estimate of the current carrying capability of the GB in the flux free state. Using this method we obtain values of up to $j_{gb} = 9 \times 10^{11}$ A/m^2 which are far above the critical value of $j_{c,gb} = 9 \times 10^{10}$ A/m^2.

As follows from a simple model of the GB, this value does not seem to be unrealistically large. A simple model of a small angle GB approximates the GB plane as a periodic array of superconducting and insulating regions.[19] Since the lattice distortions of a small-angle [001] tilt grain boundary are localized within a set of edge dislocations which induce a locally insulating area, we assume that the superconducting transport in the channels between the dislocations is not affected. Consequently, the bulk depairing current density j_0 is maintained locally in the channels and the maximum possible value of current density across the grain boundary in the flux-free state is just given by j_0 diminished by the ratio of the cross sections of the insulating dislocations to that of one of the channels. For a 4° [001] tilt boundary we obtain a distance between the dislocations of $\approx$5.5 nm and a depletion radius for superconducting properties of $\approx$1 nm.[20,21] From the resulting reduced superconducting cross section of the GB a reduction of the bulk depairing current density j_0 to a value of $j_{0,gb} \approx 2 \times 10^{12}$ is computed. This rough estimate together with our results above shows that large overcritical current densities across small angle grain boundaries are possible as long as the flux entry is prevented.

VII. SUMMARY AND CONCLUSIONS

In summary, we have shown by a combined experimental and theoretical study of superconducting strips in an asymmetric soft magnetic environment that overcritical current distributions can be obtained by field conditioning. Qualitatively, the obtained flux density distributions in our experiments agree very nicely with the ones of the theoretical model. Deviations in the values of the flux peaks at the film's edges are well understood. They are due to the modeling of the films with zero film thickness. The analysis of the field distribution of the combined system of superconductor and soft magnets allows us to clearly identify the mechanism of stabilizing the Meissner state, which is due to the diminution of the magnetic flux at the edge of the superconductor and to the concentration of the magnetic flux in the high-μ region. This mechanism renders the flow of overcritical current densities at the shielded edges of the film possible. Of significant importance is that this mechanism works also for grain boundaries. In high-T_c superconductors their critical current densities are strongly suppressed with increasing grain boundary misorientation angle and with increasing magnetic fields. The prevention of flux penetration by soft magnetic environments and the strong evidence for overcritical intergranular current densities thus open up new possibilities for improvement of critical currents in technical conductors and for the study of basic mechanisms of current transport across grain boundaries in the flux-free state.

ACKNOWLEDGMENTS

This work was supported by the Deutsche Forschungsgemeinschaft (DFG). Gratefully acknowledged is the general support by H. C. Freyhardt and discussions with R. Kress.

[1] G. Blatter, M. V. Feigelman, V. B. Geshkenbein, A. L. Larkin, and V. M. Vinokur, Rev. Mod. Phys. **66**, 1125 (1994).
[2] E. H. Brandt and M. Indenbom, Phys. Rev. B **48**, 12893 (1993).
[3] Y. A. Genenko, A. Usoskin, and H. C. Freyhardt, Phys. Rev. Lett. **83**, 3045 (1999).
[4] Y. A. Genenko, A. Snezhko, and H. C. Freyhardt, Phys. Rev. B **62**, 3453 (2000).
[5] R. Kress, *Linear Integral Equations*, 2nd ed. (Springer-Verlag, New York, 1999).
[6] H. Heese, Math. Methods Appl. Sci. **27**, 1725 (2004).
[7] H. Jarzina, Ch. Jooss, and H. C. Freyhardt, J. Appl. Phys. **91**, 3775 (2002).
[8] Y. Yeshurun, A. P. Malozemoff, F. Holtzberg, and T. R. Dinger, Phys. Rev. B **38**, 11828 (1988).
[9] A. V. Pan, S. Dou, and T. H. Johansen, *Magneto-optical Imaging*, NATO Advanced Studies Institute, Series B: Physics (Plenum, New York, 2004), Vol. 142, p. 141.
[10] A. V. Pan and S. Dou, J. Appl. Phys. **96**, 1146 (2004).
[11] M. Lange, M. J. Van Bael, Y. Bruynseraede, and V. V. Moshchalkov, Phys. Rev. Lett. **90**, 197006 (2003).
[12] Z. Yang, M. Lange, A. Volodin, R. Szymczak, and V. V. Moshchalkov, Nat. Mater. **3**, 793 (2004).
[13] E. H. Brandt, Phys. Rev. Lett. **74**, 3025 (1995).
[14] K. Guth, V. Born, and Ch. Jooss, Eur. Phys. J. B **42**, 239 (2004).
[15] Ch. Jooss, A. Forkl, R. Warthmann, and H. Kronmüller, Physica C **299**, 215 (1998).
[16] Ch. Jooss, J. Albrecht, H. Kuhn, S. Leonhardt, and H. Kronmüller, Rep. Prog. Phys. **65**, 651 (2002).
[17] V. Born, K. Guth, H. C. Freyhardt, and Ch. Jooss, Supercond. Sci. Technol. **17**, 380 (2003).
[18] A. I. Larkin and Yu. N. Ovchinnikov, Zh. Eksp. Teor. Fiz. **61**, 1221 (1971) [Sov. Phys. JETP **34**, 651 (1972)].
[19] D. Agassi, D. K. Christen, and S. J. Pennycook, Appl. Phys. Lett. **81**, 2803 (2002).
[20] Ch. Jooss, K. Guth, M. A. Schofield, M. Beleggia, and Y. Zhu, Physica C **408–410**, 443 (2004).
[21] M. A. Schofield, M. Beleggia, Y. Zhu, K. Guth, and Ch. Jooss, Phys. Rev. Lett. **92**, 195502 (2004).